

Article

Preparation and Characterization of Ag₂O Thin Films on Construction Textiles for Optoelectronics Applications: Effect of Aging on Its Optical and Structural Properties

Valentina Krylova ¹, Vaida Dobilaitė ² and Milda Jucienė ^{2,*}

¹ Faculty of Chemical Technology, Kaunas University of Technology, 50254 Kaunas, Lithuania; valentina.krylova@ktu.lt

² Institute of Architecture and Construction, Kaunas University of Technology, 44405 Kaunas, Lithuania; vaida.dobilaite@ktu.lt

* Correspondence: milda.juciene@ktu.lt

Abstract: The aim of the research was to modify the surface of construction textiles by means of the use of thin silver oxide films, investigate the structure and optical and mechanical properties, and determine the structure, optical and mechanical properties of the aged composites. Thin films of silver oxide (Ag₂O) were synthesized on a flexible PET/PVC construction textile (CT); the structural, optical, and physical properties, as well as the effect of artificial aging on these properties, were investigated. The SILAR method (successive ionic layer adsorption and reaction) was used to synthesize thin Ag₂O films on the CT surface. Before the thin films were deposited, the CT surface was mechanically roughened and pretreated with acidic and alkaline solutions at an elevated temperature. XRD analysis showed that the deposited films were a polycrystalline mixed phase material consisting of Ag₂O, AgO, and metallic Ag. Diffuse reflectance spectra in the ultraviolet and visible ranges (UV-Vis) were used to study the optical properties of the deposited thin films. The synthesized Ag₂O/CT composites were direct-gap semiconductors (the optical band gap (E_g) was 0.89 ± 0.02 eV). E_g and refractive indices (n) increased as the aging tests were carried out. Higher E_g and n meant that the composites were a good material for optoelectronic applications. The results showed that, after modification, the structural properties and tear strength of the PET/PVC fabric remained the same while the tensile strength decreased. The same tendencies remained after artificial aging.

Keywords: construction textiles; Ag₂O films; XRD analysis; optical properties; aging



Citation: Krylova, V.; Dobilaitė, V.; Jucienė, M. Preparation and Characterization of Ag₂O Thin Films on Construction Textiles for Optoelectronics Applications: Effect of Aging on Its Optical and Structural Properties. *Coatings* **2023**, *13*, 1613. <https://doi.org/10.3390/coatings13091613>

Academic Editor: Andrey V. Osipov

Received: 18 August 2023

Revised: 6 September 2023

Accepted: 11 September 2023

Published: 15 September 2023



Copyright: © 2023 by the authors. Licensee MDPI, Basel, Switzerland. This article is an open access article distributed under the terms and conditions of the Creative Commons Attribution (CC BY) license (<https://creativecommons.org/licenses/by/4.0/>).

1. Introduction

In creating facades of modern buildings, an important role is played by their design, technological-based materials, and construction methods. Textile facades provide great possibilities for architectural expression and free forms, and complex geometries are structurally possible and economically attractive [1]. The concept of textile envelope-integrated flexible photovoltaic (TE-EPV) systems has been one of the most promising forms of technology when it comes to being able to promote the development of virtually-zero energy buildings with renewable energy utilization, due to its advantageous properties [2]. To study electrical conductivity properties, a growing number of researchers have used textiles as an alternative substrate in the fabrication of nanogenerators, as textiles have many advantages such as being nontoxic, cheap, foldable, and wearable, and can be easily added to the architecture of nanogenerators [3]. Technically coated fabrics, together with additions in energy recovery, have been found to be a sustainable and prospective solution for architectural facades. One of the most promising new forms of flexible solar heat collection products that can be used for the roofs and facades of buildings is textile-based solar thermal energy collectors [4,5].

The thin films of metal chalcogenides absorb sunlight well. In [6], Ag₂S thin films were deposited by chemical bath deposition (CBD) on oxidized polypropylene. Studies have shown that films have high adsorption coefficients of approximately 10⁴ cm⁻¹ and are able to provide most of the absorption of sunlight in a thin layer. By introducing them into polymers, one can obtain composites with compatible optical and structural properties.

Another study designed and investigated a new flexible solar air heater. The core of the heater is an integrated flexible warp knit spacer fabric composite. In the composite, the intermediate filaments are coated with solar energy-absorbing materials. In addition to acting as a solar thermal energy harvesting layer, this system also provides airflow channels for energy transfer [7].

In another study, researchers used a blend of Te nanorods with Ag₂Se nanoparticles to produce high-performance thermoelectric materials. This nanocomposite presented an almost twofold increase in the efficiency of the thermoelectric materials compared to the use of pure Ag₂Se nanoparticles [8].

Another study developed a sustainable strategy for the scalable production of α-Fe₂O₃ nanocrystals with 3D interconnected porous architectures on flexible carbon textiles (CTs). It was found that LIBs, which were based on recycled Fe₂O₃@CTs, exhibited electrochemical performance levels with no decay when compared to the results from a format based on the use of fresh products [9].

Using a simple CBD method, the researchers obtained and studied hierarchical porous NiO nanoflake arrays on carbon fabrics. Free-standing NiO nanoflakes with a thickness of ~10 nm quasi-vertically grew to the carbon cloth, forming an integrated flexible electrode. The nanoflake array electrode exhibited electrochemical performances with high capacitance and a desirable high-rate cycle life (with 82% retention after 4000 cycles) [10].

Another study [11] also used a CBD method for nanocrystalline Ag₂Se thin film depositions on transparent polyester sheets. According to the authors, the thin films of Ag₂Se could be used in solar energy equipment and optoelectronics.

The real application of architectural textile-based solar energy materials is challenging because of the poor adhesion of the coating film to the substrate. In one study [12], the effect of thermochemical pre-treatment on the surface properties of textiles was analyzed to evaluate their applicability for the deposition of semiconductor materials requiring high surface hydrophilicity. These researchers also synthesized AgInSe₂ semiconductor films on pre-treated textiles using CBD and sequential adsorption and ion layer reaction (SILAR) methods to investigate their optical properties [13].

Oxides with semiconductor properties have been used for many years in photovoltaic (PV) forms of technology. The versatility of their properties and the simplicity of their production methods give oxides a unique position in relation to the new generation of PV. Their ability to maintain or improve electronic performance allows them to be used in flexible photovoltaic equipment [14]. Metal oxides come in various shapes and sizes, are stable at ambient temperature and in the surrounding air, and are generally harmless to living organisms. Many metal oxides are n-type semiconductors. Known p-type oxides include copper (I) oxide, nickel (II) oxide, and silver (I) oxide. Use could be made of p-type oxides to form oxide heterojunctions in solar cells. The rationale in singling out silver oxide rather than other cost-effective metal oxides, for example, copper oxide, is determined by its thermodynamic stability and the possibility of synthesis at ambient temperature. Copper oxide is relatively cheap and relatively stable in terms of both chemical and physical properties, but its synthesis by chemical methods from Cu(OH)₂ (analogically as from AgOH) occurs at high temperatures. The pure Cu(OH)₂ can stay for several months in pure water at room temperature, without being transformed into CuO. However, a slow transformation is thermodynamically possible because the solubility found in pure water is more important for Cu(OH)₂ (1.3 × 10⁻⁵ mol/dm³) than for CuO (2 × 10⁻⁷ mol/dm³) [15]. Copper hydroxide has a complex decomposition as it is heated. Only at about 185 °C does it decompose to heat-stable CuO [16], while the construction textile remains stable up to 70 °C. Accordingly, high temperatures are required for the formation of other oxides.

Various phases of silver oxide have been reported [17], of which Ag₂O is the most thermodynamically stable [18]. Thin silver oxide films can be prepared using various techniques, including chemical bath deposition [19], electrodeposition [20], pulsed laser deposition [21], magnetron sputtering [22,23], electron beam evaporation [24], and more. In the currently available literature, the optical band gap for Ag₂O varies from 1.2 eV [25] to 3.4 eV [26]. The range depends on the stoichiometry, as well as the structure and physical properties that result from the deposition method.

For mixed phases (AgO and Ag₂O), the stated values of the band gap tend to lay within the range of 2.4 eV to 2.7 eV [22]. This range covers several photovoltaic applications, from 1.4 eV band-gap absorbers for solar cells to transparent conductive oxides with a band gap greater than 3 eV. The abundant silver oxide phases and the lack of a detailed analysis of the crystal structure are most likely the main reasons for the wide range of reported band gap values [26].

For this study, silver oxide films were prepared by means of the use of the SILAR method. Due to its low cost and simplicity, this method is widely used by scientists [27].

In the study, the researchers found that, compared to standard Co-based selective solar absorbers, if the emittance of the investigated system is within the range of those exhibited by Co–Al₂O₃, Co₃O₄/Co, and Ni–Co₃O₄/Co systems, its absorptance is superior. In this investigation, the ultrafast surface-structured Co nanocylinders in the Alumina host matrix exhibited an optical absorptance $\alpha(\lambda)$ above 98% and a relatively low emittance $\epsilon(\lambda)$ of 0.03 in the spectral solar range of 200–1100 nm [28].

In other research, it has been shown that, for modified samples of thin films, an increase in the rate constant of the decomposition reaction is 2–4.5 times higher than in the initial samples. The degree of mineralization was up to 90%. Cyclic tests showed that an increase in the number of cycles led to an increase in the adsorption of dye decomposition products on the thin film surface and a subsequent decrease in the photocatalytic activity and degree of mineralization of investigated samples. For irradiated samples of thin films, this decrease was much smaller and amounted to no more than 5–15% for the degree of photocatalytic decomposition, and 25–30% for the degree of mineralization [29].

The base material of the constructional textile for outdoor application is coated and lacquered; the main purpose of the coating is to protect the fabric and provide desirable properties. Thermochemical modification processes may affect the upper layer, causing it to lose its protective properties, as specified in the technical specification. Although preliminary studies have shown [12] that, after the thermochemical treatment of architectural textiles, the change in strength is not significant; attention should be paid to the exploitation conditions of this material. A constructional textile for membrane facades is exposed to high and low temperatures, humidity, solar heat, ultraviolet rays, wind load, and other harmful factors of the natural environment [30]. Studies conducted under both natural and artificial aging conditions show that, due to climate factors, the color of architectural membranes changes, and their mechanical properties, such as strength, elasticity, stiffness, and tear resistance, decrease [31–38]. It should be noted that changes are usually not caused by single factors, but by a combination of effects; thus, more factors are included in the test protocol for artificial aging, and harder, more intensive conditions are created, such as longer exposure time or sample loading. An analysis of the scientific literature on the aging of coating materials for membrane structures confirmed that it is relevant to conduct research aimed at evaluating the variation of technical properties of thermochemically treated constructional textiles, taking into account environmental factors, both from the point of view of the stability of these materials' properties and their commercial viability.

The aim of the research is to modify the surface of construction textiles by means of the use of thin silver oxide films, investigate the structure and optical and mechanical properties, and determine the structure and optical and mechanical properties of the aged composites.

2. Experimental

2.1. Materials

A selection was made for the purposes of this study of PET/PVC coating material for textile buildings (Table 1). According to the manufacturer (Verseidag-Indutex GmbH, Krefeld, Germany), this meets the requirements for membrane structures, while also being durable, light, flammable, and easy and economical to maintain.

Table 1. Specifications of the test material.

Support Cloth *	Coating *	Thickness, mm	Total Weight, g/m ²	Adhesion,* N/5 cm	Application *
Polyester Fabric	PVC both sides lacquered and one-side PVDF	0.56	720	100	construction textile structures

* Producer specifications.

The reagents used to prepare the reaction solutions were as follows: sodium hydroxide (NaOH, >98%, Sigma-Aldrich Chemie GmbH, Munich, Germany), chromium(VI) oxide (CrO₃, ≥97.0%, Reachim Ltd., Moscow, Russia), sulphuric acid (H₂SO₄, ≥96%, Barta a Cihlar, Rožnov pod Radhoštěm, Czech Republic), orthophosphoric acid (H₃PO₄, ≥60%, Lach-Ner, Ltd., Neratovice, Czech Republic), and silver nitrate (AgNO₃, ≥99.0%, Sigma-Aldrich Chemie GmbH, Munich, Germany). The deposition process parameters for these thin films—such as chemical concentration, pH, reaction temperature, and reaction time—were optimized by repeating the experiment multiple times until a good quality thin film could be obtained.

2.2. Experimental Setup

The scope of the research (Figure 1) includes the surface modification of pre-treated construction textiles using thin films of silver oxide by chemical deposition, as well as the study of their structural, optical, technical, and mechanical properties. Before depositing silver oxide films, the textile was pretreated in two different ways according to the procedure detailed in our previous work [12]. Furthermore, the influence of climatic exposure was investigated during artificial accelerated aging. These tests were included in the analysis, taking into account the fact that construction textiles cover large parts of building exteriors and are subjected to changing climatic stresses, so it is relevant to accumulate knowledge about the performance properties of construction textiles with the Ag₂O layer. During accelerated aging, the effects of humidity, heat, and cold were simulated in two different ways with different exposure intensities (as described in Section 2.2.2).

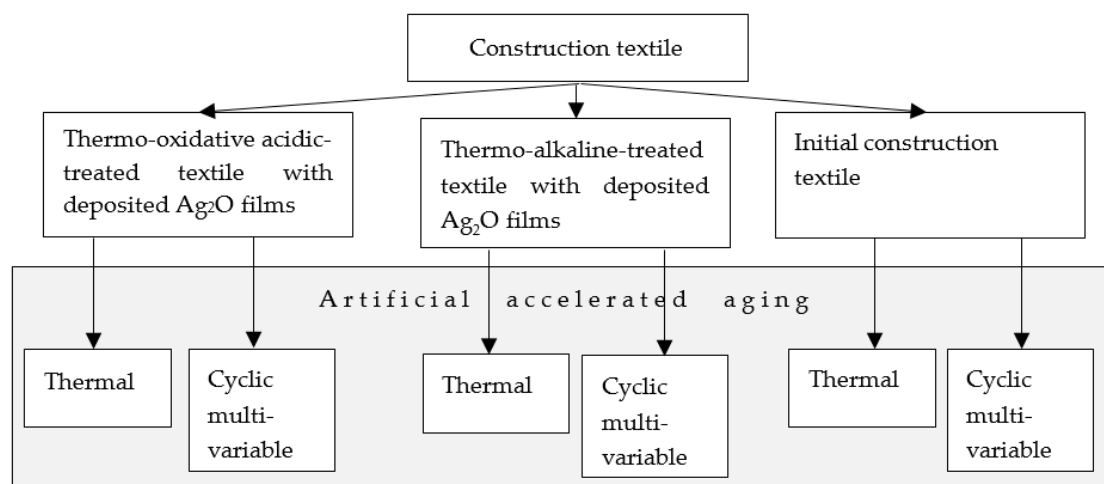


Figure 1. Stages of experimental research.

2.2.1. Ag₂O Film Deposition on Construction Textiles Stages Mechanical Roughening of the Surface

The main stages of the surface modification process through the use of silver oxide thin films for construction textiles are shown in Figure 2. The surface of the construction textiles is covered with a layer of lacquer, the main purpose of which is to protect the material from environmental factors (UV radiation, humidity, and temperature changes). The first stage of modification involves the mechanical roughening of the surface of the material. The roughening was mechanically carried out using SiO₂ sanding paper, P180, for smooth roughening (according to FEPA Standard 43-1) and keeping the number of scrub cycles and the pressure of any downward force constant. The minimum number ($n = 5$) of scrub cycles was selected to damage the lacquer coating alone. During the course of the test, the face side of the sample was affected by the abrasive, and the effect of the roughened abrasive was visually assessed. A comparison of the loss in gloss with that of an unused comparison piece was selected as the main criterion for the means of any evaluation process. Following the mechanical roughening stage, the samples were washed with running water and then distilled water to remove any dirt, abrasives, and broken particles of polymers that may still have been adhering to the surface.

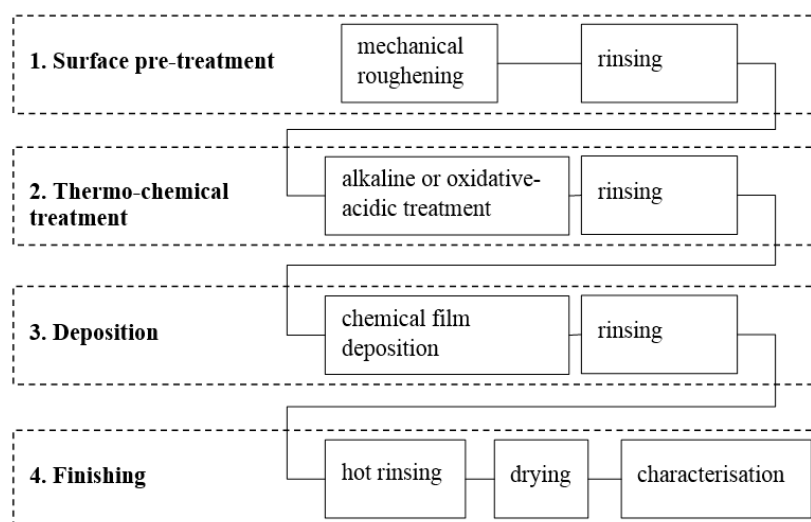


Figure 2. Various steps in the surface modification process of construction textiles.

Pre-Treatment of the Textile Surface

The thermochemical surface treatment was performed by exposing the samples to two different solutions for 90 min. It is important that polymer degradation should be avoided to ensure the successful modification of the polymer surface. As a rule, the temperature changes from 20 °C to 80 °C [39–41] in alkaline pre-treatment; while in acid pretreatment processes, the working temperature is typically at least 80 °C [12,42]. The manufacturer recommended that the construction textile remain stable up to 70 °C; regarding this, a temperature of 65 ± 1 °C was selected for these experiments. The oxidative acidic treatment was carried out in a solution that was mixed with 7.2 M H₂SO₄, 6.6 M H₃PO₄, and 0.36 M CrO₃, with an alkaline treatment that involved a 4.2 M NaOH solution. Treatments were carried out in a glass container with a volume of 2 dm³ (Figure 3). After completion of the thermochemical treatments, samples were repeatedly washed with hot water. Finally, before thin films were deposited in place, test samples were rinsed with distilled water (until pH ~7 was reached) and then conditioned in air at room temperature.



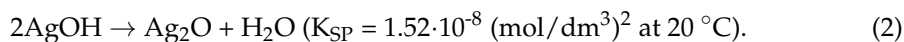
Figure 3. Photograph of the reaction container with the samples.

Ag₂O Synthesis

Ag₂O can be synthesized by combining aqueous AgNO₃ and NaOH solutions:



This reaction does not produce any appreciable amount of AgOH due to the favorable energy for the next reaction [43]:



Under properly controlled conditions, this reaction can be used to produce Ag₂O with properties suitable for several applications, including as fine-grained conductive thin films:



Ag₂O layers were deposited by employing the SILAR method at room temperature. For this task, prepared samples were vertically placed in a glass reactor with a 0.1 M AgNO₃ solution and left undisturbed for 6 h. After this time had passed, the test samples were removed, washed with running water and then distilled water, and exposed to a 0.35 M NaOH solution for 6 h. Sample immersion in AgNO₃ and subsequent immersion in the NaOH solution formed one Ag₂O preparation cycle. In summary, six cycles were used. The samples obtained were cleaned, dried, and then characterized.

The view of the mechanically roughened and pretreated samples with deposited Ag₂O films is presented in Figure 4. The labeling of treated and untreated samples is listed in Table 2.

Table 2. Sample labeling.

Labelling	Schedule
CT	construction textile
Ag ₂ O/CT-TOAc	construction textiles after thermo-oxidative acid treatment with deposited films of Ag ₂ O
Ag ₂ O/CT-TA	construction textiles after thermo-alkaline treatment with deposited films of Ag ₂ O

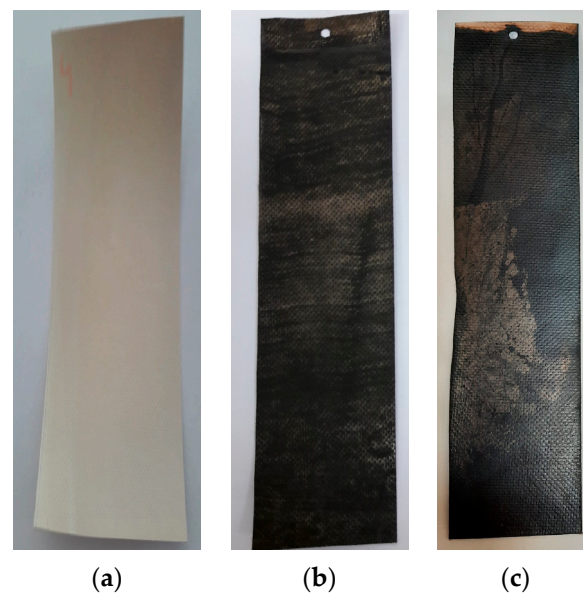


Figure 4. Samples used for the tests: (a) roughened CT side; (b) $\text{Ag}_2\text{O}/\text{CT-TA}$; and (c) $\text{Ag}_2\text{O}/\text{CT-TOAc}$.

2.2.2. Accelerated Aging Tests for Initial CT and CT with Deposited Ag_2O Layer

To investigate changes in the structural, optical, and mechanical properties of CT, $\text{Ag}_2\text{O}/\text{CT-TOAc}$, and $\text{Ag}_2\text{O}/\text{CT-TA}$ after exposure to various destructive factors, accelerated aging of the test samples was carried out using two different methods. Specifically, thermal aging and cyclic multivariable aging were performed in the laboratory. According to the first method, one group of test samples was subjected to hot air at a temperature of $70\text{ }^\circ\text{C}$ and an atmospheric pressure for 336 h. Such aging conditions are provided in the ISO 1419:2019 standard (method B) [44]. The second artificial aging method is designed considering climatic factors characteristic of the continental climate zone of mid-latitude by distinguishing a smaller area characterized by moderately warm summers and moderately cold winters, as well as occasional tropical and Arctic weather conditions. In the second model, such conditions are simulated by including humidity, high- and low-temperature factors, and cyclically applying their exposure. One cycle consists of the full immersion of the samples in ambient temperature water ($23 \pm 2\text{ }^\circ\text{C}$) for 24 h, then exposed to cold ($-18 \pm 3\text{ }^\circ\text{C}$) for 24 h and dry heat ($70 \pm 3\text{ }^\circ\text{C}$) for 48 h. During the study, five cycles were performed for the samples from the second group, giving a total exposure time of 480 h. The test equipment was a laboratory bath for immersion, a RUMED cooling chamber Type 3301 (Rubarth Apparate GmbH, Laatzen, Germany) for freezing, and a ventilated chamber SNOL 58/350 (SnolTherm, Utena, Lithuania) for heating. After aging according to both methods, the test samples were placed at a temperature of $(23 \pm 2)\text{ }^\circ\text{C}$ and a relative humidity of $(50 \pm 5)\%$ for conditioning, then their structural, optical, and mechanical properties were determined and the data were compared with the properties of the unaged test samples.

2.3. Characterization

XRD phase analysis of the samples was carried out on a D8 Advance diffractometer (Bruker AXS, Karlsruhe, Germany), in the range $2\theta = 3\text{--}70^\circ$. The operating parameters are detailed in [12].

A Lambda 35 UV visible spectrophotometer (Perkin Elmer Inc., Waltham, MA, USA) was used to record UV-Vis diffuse reflectance spectra (R_d).

Wavelength-dispersed X-ray fluorescence (XRF) data were obtained using a S8 Tiger spectrometer (Bruker AXS, Karlsruhe, Germany). The operating parameters are described in detail in [33].

The thickness T (mm) of the samples was measured according to the standard ISO 2286–3 [45]. The total mass per unit area W (g/m^2) was determined according to the standard ISO 2286–2 [46]. A tear and tensile test was carried out to investigate the influence of thermochemical treatment and aging on the mechanical characteristics of the fabric being investigated. The tensile strength was determined according to standard EN ISO 1421 [47], and tear strength was determined according to standard EN 1875–3 [48]. A set of test pieces were cut in two directions (longitudinal and transverse) for both experiments. The samples were conditioned as specified in ISO 2231 [49] (atmosphere B; $(23 \pm 2)^\circ\text{C}$ temperature, and $(50 \pm 5)\%$ relative humidity) before the mechanical test was carried out. Additionally, these conditions were retained during the experiments. The universal testing machine BTI-FB050TN (ZwickRoell GmbH & Co, Ulm, Germany), provided with a 5 kN load cell and a grip width of >50 mm, was used to carry out the mechanical test. The data obtained had to be statistically processed, by calculating the standard deviation and the coefficient of variation.

The effect of pretreatment and aging on the strength of CT was evaluated by means of a reduction factor, A_t , which was calculated as the ratio of the tensile strength of the initial and pretreated and aged test samples.

3. Results and Discussion

3.1. Investigations of Ag_2O Films on CT before Accelerated Aging Tests

3.1.1. XRD Analysis

The structure and phase purity of the CT samples before and after thermochemical treatment and the process of depositing thin silver oxide films were examined by XRD; the patterns are shown in Figure 5. In an X-ray diffractogram of the CT sample (Figure 5a), the peaks of polyvinylchloride (PVC) and polyethylene terephthalate (PET) are observed at $2\theta = 18.69^\circ$ and 25.70° . In addition, characteristic peaks are observed corresponding to the (110), (101), (200), (211), (220), and (301) crystal planes of the tetragonal phase of rutile (TiO_2) (PDF No. 04-006-1890), and to crystal planes (104), (113), (202), (016), and (018) of the rhombohedral phase of calcite (CaCO_3) (PDF No. 05-0586).

The XRD patterns for the resulting $\text{Ag}_2\text{O}/\text{CT}$ composites do not strongly depend upon the pretreatment solution. As can be seen (Figure 5b), the XRD patterns from $\text{Ag}_2\text{O}/\text{CT}-\text{TOAc}$ composites resulted in several new diffraction peaks at $2\theta = 32.70^\circ$, 34.76° , 37.90° , 45.67° , 54.34° , and 65.49° , respectively. The diffraction peaks at $2\theta = 32.70^\circ$, 37.90° , and 65.49° were related to (111), (200), and (311) Bragg reflections of bulk Ag_2O (PDF No. 12-0793) with a cubic structure [50].

The peak for silver oxide at $2\theta = 54.34^\circ$ (220) can overlap with the TiO_2 peak at $2\theta = 54.42^\circ$. The peak at $2\theta = 34.76^\circ$ is related to monoclinic AgO (111) (PDF No. 84-1547) [51]. The diffraction peak for silver is located at $2\theta = 44.30^\circ$ (200) (PDF No. 04-003-1472). The new peak at $2\theta = 45.67^\circ$ could be due to the existence of a cubic phase from silver nanoparticles, or it could be associated with the formation of a mixed $\text{Ag}/\text{Ag}_2\text{O}$ phase, as reported in [52].

The XRD results from $\text{Ag}_2\text{O}/\text{CT}-\text{TA}$ composites (Figure 5c) resulted in the creation of the same multiple new diffraction peaks at $2\theta = 32.62^\circ$, 34.74° , 37.75° , 45.61° , 54.60° , and 65.37° . A slight shift in the diffraction peaks (111), (200), and (311) for Ag_2O was noted at the 2θ angle, 32.62° , 37.75° , and 65.37° , respectively. The diffraction peak at $2\theta = 34.74^\circ$ could be indexed as monoclinic AgO (111), and the diffraction peak located at $2\theta = 45.61^\circ$ could be indexed as (200) planes metallic silver, or it could be associated with the mixed-phase for $\text{Ag}/\text{Ag}_2\text{O}$ [52,53]. The peak at $2\theta = 54.60^\circ$ can be indexed as Ag_2O (220) and/or assigned to the TiO_2 peak.

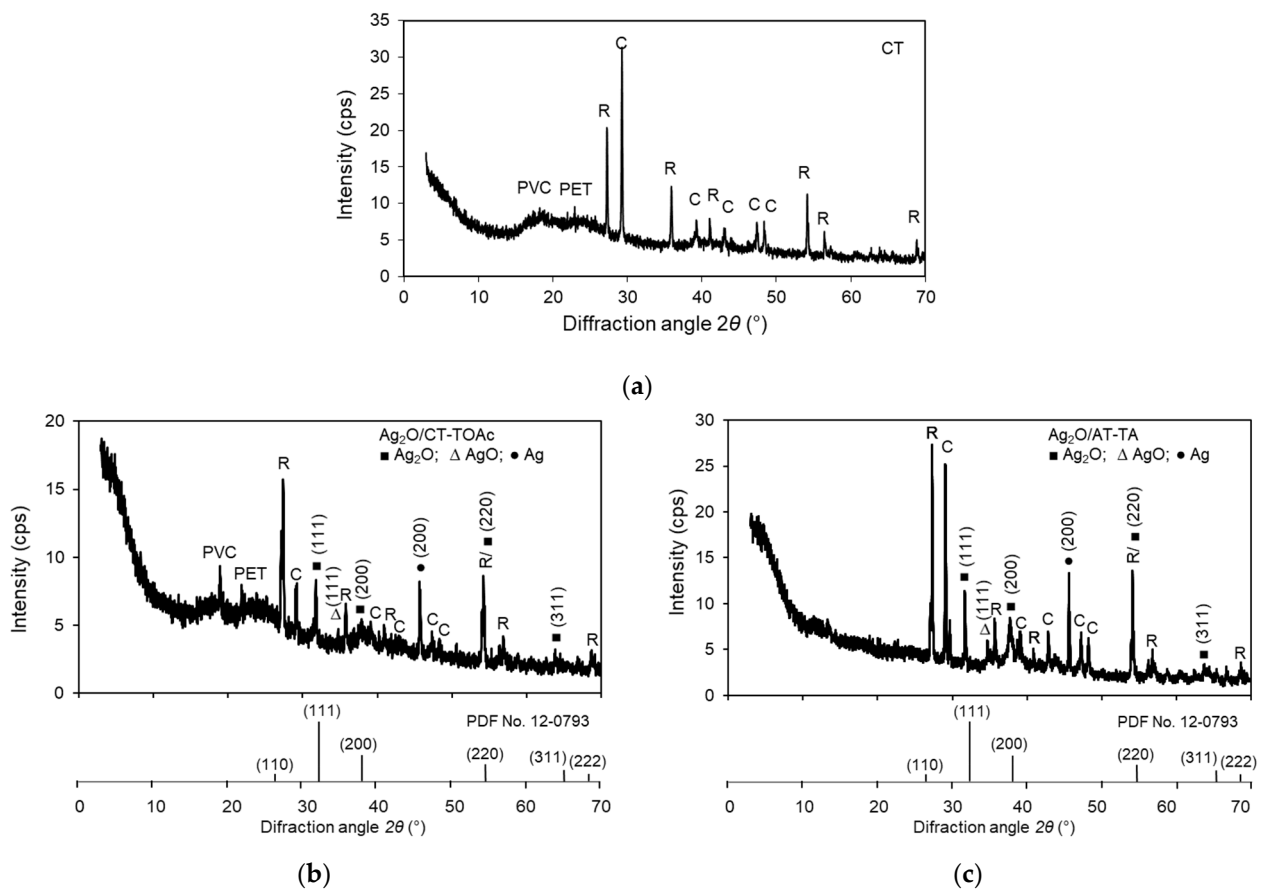


Figure 5. XRD patterns of the CT (a), $\text{Ag}_2\text{O}/\text{CT-TOAc}$ (b), and $\text{Ag}_2\text{O}/\text{CT-TA}$ (c) composites. Indexes: C—calcite, R—rutile, PET—polyethylene terephthalate, PVC—polyvinylchloride, when ■ is Ag_2O , Δ is AgO , and ● is Ag.

For $\text{Ag}_2\text{O}/\text{CT-TA}$ composites, the intensity of Ag_2O (111) and (200) reflections increased, indicating the fact that crystallinity levels had increased in the Ag_2O films. These results suggest that silver oxide films grown on pretreated CT are polycrystalline.

An analysis of the XRD patterns of the CT and the obtained composites shows a change in the intensity and position of the diffraction peaks corresponding to both organic substituents and inorganic fillers, as well as the deposited films, depending on the thermochemical pretreatment of CT in various solutions. In the $\text{Ag}_2\text{O}/\text{CT-TOAc}$ composites, a noticeable decrease in the intensity of the diffraction peaks is observed compared to the XRD pattern of the $\text{Ag}_2\text{O}/\text{CT-TA}$ sample, indicating a deterioration in the crystalline quality of the inorganic components. Analysis of the XRD patterns shows that inorganic compounds are more stable on textiles treated with a thermo-alkaline solution.

3.1.2. UV-Vis Analysis

The R_d spectra of the CT and Ag_2O films on different pretreated CTs are all shown in Figure 5. The reflectivity of CT sharply increases from 60% to 92%, in the region from 400 nm to 430 nm. Then, it reaches an almost constant value of about 97% in the region from 647 nm to 1020 nm (Figure 5). From 1020 nm to 1100 nm, reflectivity increases up to 99%. Such a relatively high reflectance indicates that CT reflects solar radiation. CT reflects in two spectra: near-infrared and visible.

A noticeable drop in the intensity of the reflection is rather obvious in the $\text{Ag}_2\text{O}/\text{CT-TOAc}$ and $\text{Ag}_2\text{O}/\text{CT-TA}$ spectra in a wide range of the electromagnetic spectrum, from 400 nm to 1100 nm (Figure 5). The reflection intensity in this interval is almost constant, amounting to about 59–54%.

The optical band gap (E_g) was determined using Equations (4) and (5) [54,55]:

$$F(R) = \frac{(1 - R)^2}{2 \cdot R}, \tag{4}$$

$$hvF \sim (hv - E_g)^n, \tag{5}$$

where F is the Kubelka-Munk function, hv is the photon energy, R is the reflectance, E_g is the optical band gap, while n depends on the interband transition mechanism.

Crystalline materials, in most cases, form an allowed direct transition, whereas, for semiconductor amorphous materials, there is a possibility of an allowed indirect transition. For the allowed direct transitions $n = 2$, the experimental data contain a long straight line on the plot of $(hvF)^2$ versus hv (Figure 6).

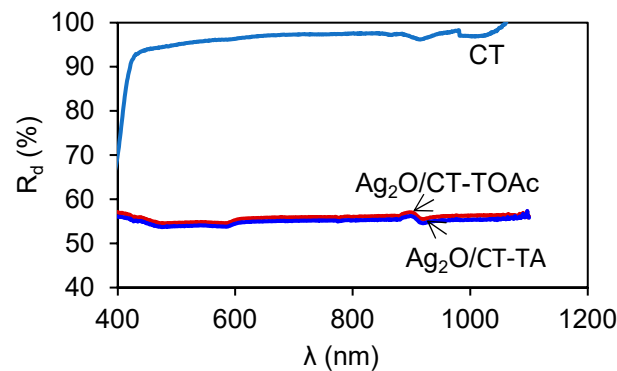


Figure 6. Measured R_d spectra of CT and Ag_2O films deposited on different pretreated CT.

The E_g determination from R_d spectra by means of the Kubelka-Munk method is shown in Figure 7. Ag_2O films are direct-gap semiconductors. The band gap energy is in the near-infrared region. The values obtained are given in Table 3.

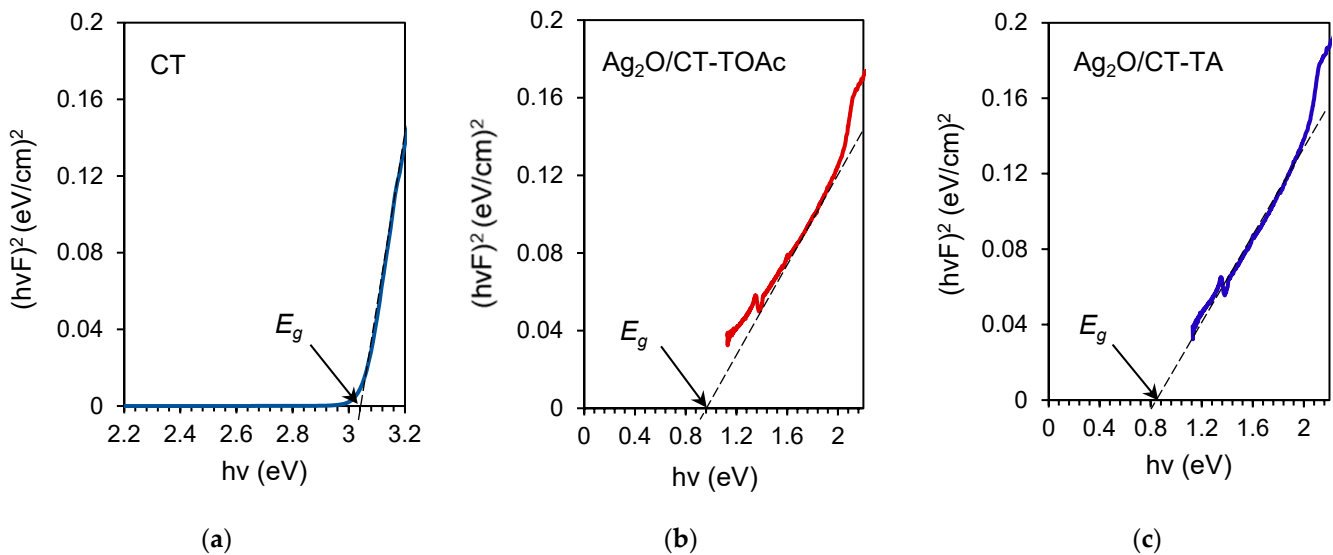


Figure 7. E_g determination from R_d spectra by means of the Kubelka-Munk method.

Table 3. Composition, obtained through XRF analysis, along with the values of the E_g and n of CT and the obtained composites.

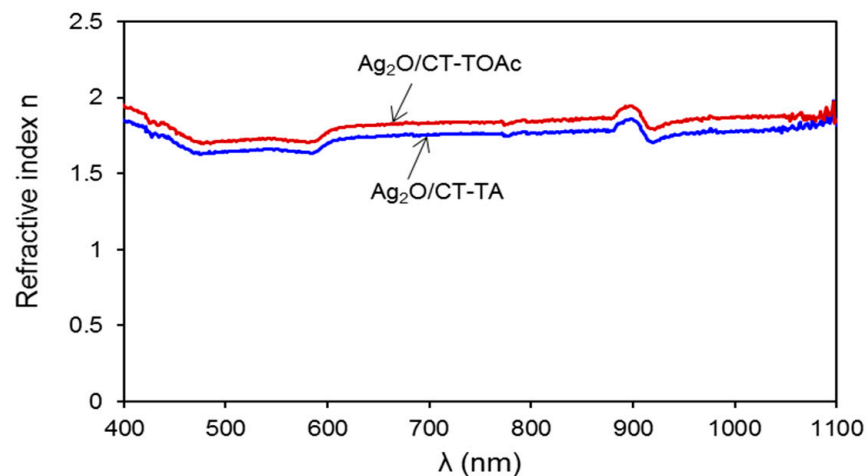
Sample	Composition, wt %				E_g , eV	n
	Cl	TiO ₂	CaO	Ag		
CT	61.70	6.66	6.20	-	3.05 ± 0.01	-
Ag ₂ O/CT-TOAc	43.90	4.03	2.62	0.57	0.89 ± 0.02	1.70–1.97
Ag ₂ O/CT-TA	31.25	2.75	6.00	0.34	0.89 ± 0.02	1.63–1.87

For commercial CT, the E_g is 3.05 ± 0.01 eV. The optical band gap values of the obtained Ag₂O/CT-TOAc and Ag₂O/CT-TA composites are the same, at 0.89 ± 0.02 eV. When comparing this against research carried out by other researchers, it can be noticed that E_g is observed to be within the range of 1.01–0.93 eV [56], otherwise it is within 1.64–1.95 eV [19]; values of 1.2 eV [25] and 3.5 eV [57] have also been found. This wide disparity in values comes as a result of varying stoichiometry, which results from different depositions.

The refractive indices (n) can be calculated using the following relationship [58]:

$$n = \frac{-(R + 1) \pm 2\sqrt{R}}{R - 1} \quad (6)$$

The spectra variation of n for thin Ag₂O films on CT within the 400–1100 nm wavelength range is shown in Figure 8.

**Figure 8.** The dependence of refractive indices for Ag₂O films on the CT surface in terms of wavelength.

The refractive indices for Ag₂O films on the CT surface are shown in Table 4. The refractive indices of the obtained composites are almost constant over the entire range of the visible and near-infrared spectra range. Various materials, including PET, PVC, TiO₂, CaCO₃, and Ag₂O, are included in the Ag₂O/CT composites. The majority of the conventional polymers reveal n , which are between 1.3 and 1.7 [59]. The values of the main refractive indices in terms of the construction textile components and precipitated silver oxide are shown in Table 4.

Table 4. Values of the main refractive indices of construction textile components and deposited silver oxide films.

Material	Refractive Index n	References
PVC	1.49–1.60	[60,61]
PET	1.55–1.64	[60,62]
TiO ₂	2.31–3.17	[63]
CaCO ₃	1.62–1.88	[64]
Ag ₂ O	1.02–2.70	[19,65]

Data on n thin Ag₂O films are absent in most of the currently available literature. For Ag₂O films deposited by DC magnetron sputtering, the obtained value of n is in the range 1.186–1.204 [65]. In other work [19], the range for the refractive index in terms of silver oxide, which was deposited on a glass slide by means of the CBD technique, was seen to be between 1.02 to 2.07, although the final readings depended upon the film deposition time [56]. Due to differences in free electron density levels, n for each of these materials is different (Table 4), so the n for a multiphase material cannot be predicted from any interpolation of the corresponding refractive indices in the pure phases. The range of refractive indices values, which have been obtained, indicates possible applications in optical non-volatile memories or optical waveguides, or integration into improved efficiency solar cells.

3.2. Investigations of Ag₂O Films on CT after Accelerated Aging Tests

3.2.1. XRD Analysis

XRD has been used to understand the phase change of silver oxide films and their crystalline structure during accelerated aging tests of the synthesized composites. The XRD data provide information about the composites in terms of peak, intensity, and position. The position of the peak indicates the symmetry of the contributing phase, the crystal structure. The intensity of the peak reflects the total scattering from each plane of the crystal and depends on the distribution of atoms in the crystal structure. Thermal vibrations of atoms in a lattice site affect the intensity of the diffracted beam. In the case of polycrystalline samples, which are the composites under study, in addition to structural and temperature factors, the peak intensity is affected by polarization, the multiplicity factor, the Lorentz factor, and the absorption coefficient. If the crystalline nature increases, the number of planes oriented in a certain direction increases and, therefore, the multiplicity increases, resulting in an increase in intensity [66]. The XRD pattern of the samples is shown in Figures 9 and 10.

After the thermal aging test (Figure 9a,b), compared to the X-ray patterns before thermal aging (Figure 5), the position of the peaks did not change, and the intensity of many reflections increased, indicating an increase in the crystallinity of both the construction textile matrix and the deposited films. The composition of Ag₂O/CT-TOAc and Ag₂O/CT-TA samples does not change. A sharp increase in crystallinity was associated with the prolonged exposure of samples at elevated temperatures.

After a cyclic multi-variable aging test of the Ag₂O/CT-TOAc composite, the Ag₂O (200) reflection intensity sharply increased (Figure 10a), which indicated an increase in the crystallinity of the Ag₂O films. For the Ag₂O/CT-TA composite, the intensity of the (110) crystal planes of the tetragonal rutile phase significantly increased, while the intensity of the (104) crystal planes of the calcite phase decreased (Figure 10b). No significant change in the intensity of other peaks was observed. Peaks of other compounds were not detected, which indicates that the purity of the deposited films did not change. After the samples were tested for aging, the XRD curve remained practically unchanged. The diffraction peaks were neither shifted nor broadened. Therefore, we can conclude that the composition of the

films did not change. The higher intensity of the peaks might be related to the positional ordering of the crystals.

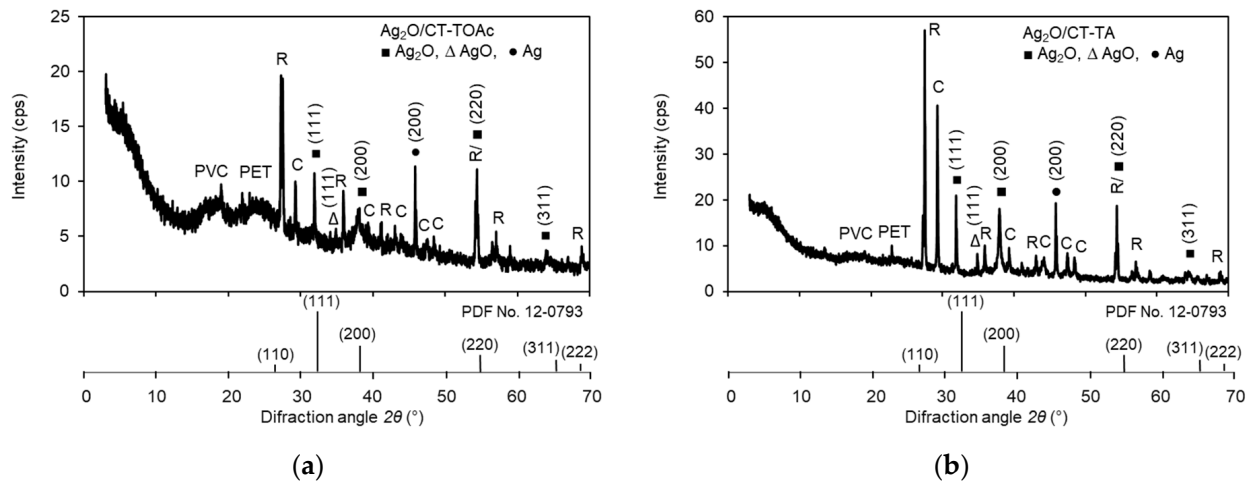


Figure 9. XRD patterns of the $\text{Ag}_2\text{O}/\text{CT-TOAc}$ (a) and $\text{Ag}_2\text{O}/\text{CT-TA}$ (b) composites after thermal aging. Indexes: C—calcite, R—rutile, PET—polyethylene terephthalate, PVC—polyvinylchloride, when ■ is Ag_2O , Δ is AgO , and • is Ag.

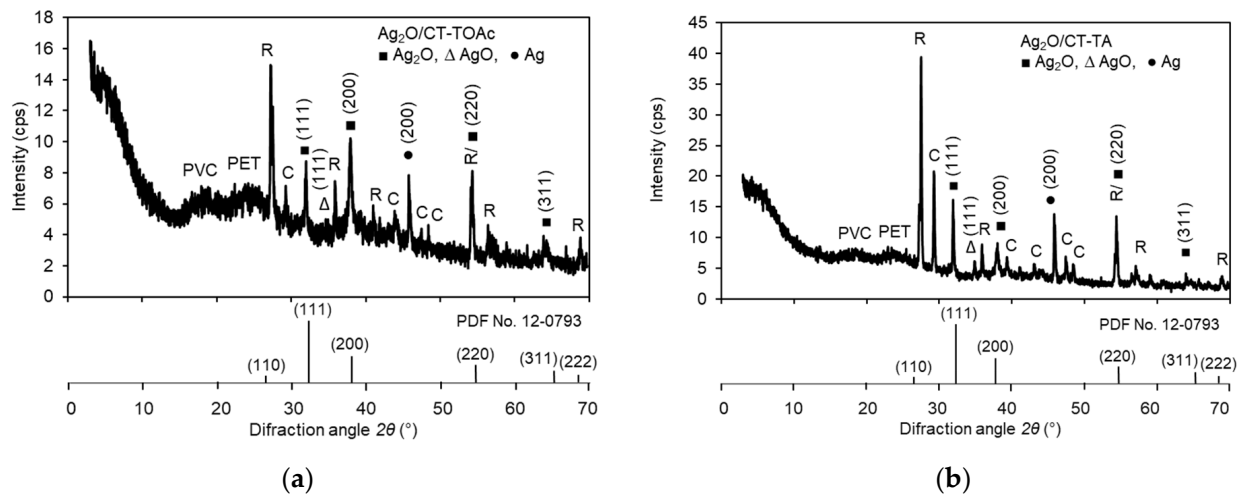


Figure 10. XRD patterns of the $\text{Ag}_2\text{O}/\text{CT-TOAc}$ (a) and $\text{Ag}_2\text{O}/\text{CT-TA}$ (b) composites after cyclic multi-variable aging. Indexes: C—calcite, R—rutile, PET—polyethylene terephthalate, PVC—polyvinylchloride, when ■ is Ag_2O , Δ is AgO , and • is Ag.

3.2.2. UV-Vis Analysis

The UV-Vis measured R_d spectra of the Ag_2O films on CT after cyclic multi-variable aging and thermal aging are all shown in Figure 11. As can be seen, after cyclic multi-variable aging, the reflection intensity in the interval from 400 nm to 1100 nm decreased from 59–54% to 38–48% and was almost the same for the $\text{Ag}_2\text{O}/\text{CT-TOAc}$ and $\text{Ag}_2\text{O}/\text{CT-TA}$ samples. After thermal aging, the reflection intensity also dropped to around 38–45%.

The optical band gap E_g values determined from diffuse reflectance spectra in the UV-visible region using the Kubelka-Munk method (Figure 12) are given in Table 5.

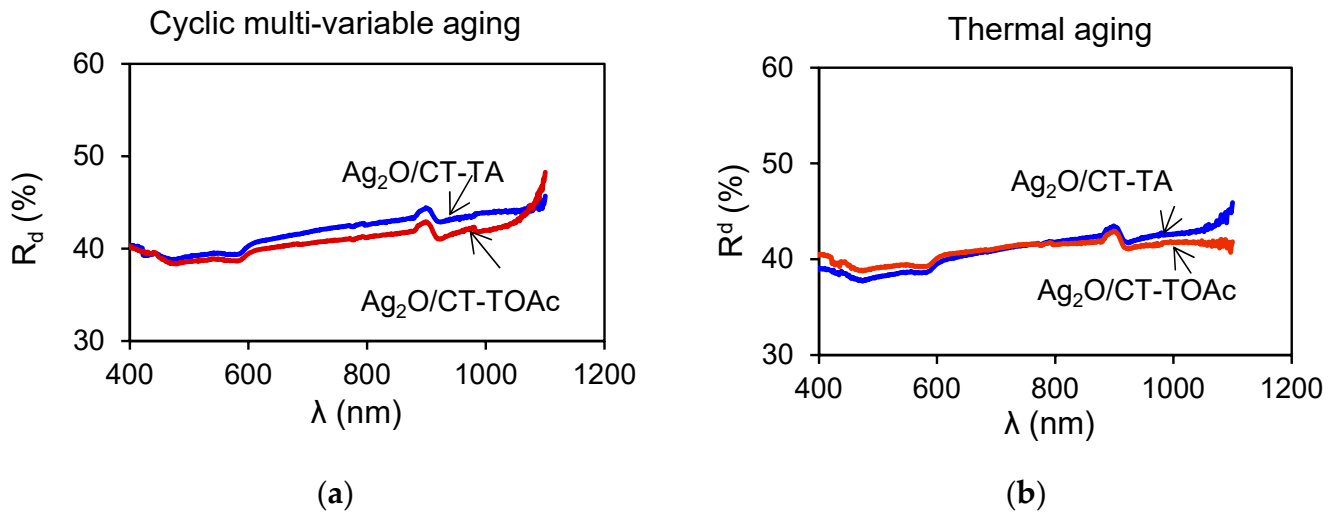


Figure 11. Measured R_d spectra of the Ag_2O films deposited on different pre-treated CT after cyclic multi-variable and thermal aging.

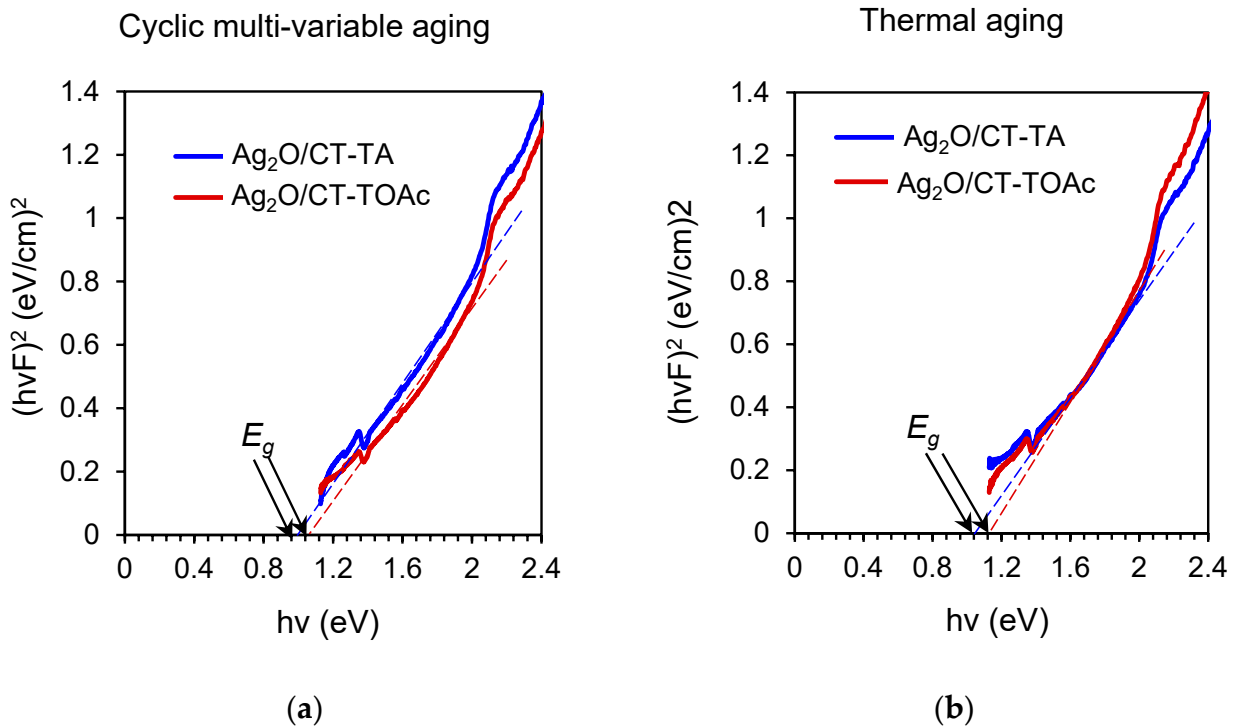


Figure 12. E_g determination from R_d spectra by means of the Kubelka-Munk method after cyclic multi-variable and thermal aging.

Table 5. The values of the E_g and n of Ag_2O films on the CT surface after accelerated aging tests.

Sample	Before Aging Test		Thermal Aging		Cyclic Multi-Variable Aging	
	E_g , eV	n	E_g , eV	n	E_g , eV	n
$Ag_2O/CT-TOAc$	0.89 ± 0.02	1.70–1.97	1.12 ± 0.02	2.27–2.51	1.20 ± 0.02	2.28–2.87
$Ag_2O/CT-TA$	0.89 ± 0.02	1.63–1.87	1.04 ± 0.02	2.28–2.70	1.12 ± 0.02	2.27–2.68

After accelerated aging tests, the E_g values of the obtained $Ag_2O/CT-TOAc$ and $Ag_2O/CT-TA$ composites increased (Table 5). When comparing the obtained results, it is evident that after cyclic multi-variable aging for both composites, the values of the E_g increase more than after thermal aging. This discrepancy in values results from their

different stoichiometry, which is the result of different processing of the construction textiles prior to the deposition of the silver oxide films. $\text{Ag}_2\text{O}/\text{CT-TA}$ composites, before the aging test, have an E_g of 0.89 eV, which shifts to 1.04 eV after thermal aging and to 1.12 eV after cyclic multi-variable aging. Thus, the E_g shift is observed in the composites, but with different values, 15 and 23 meV, respectively. In $\text{Ag}_2\text{O}/\text{CT-TO-Ac}$ composites, E_g shifts from the same 0.89 eV to 1.12 eV after thermal aging and to 1.20 eV after cyclic multi-variable aging. Thus, the E_g shift is also observed in the $\text{Ag}_2\text{O}/\text{CT-TO-Ac}$ composites, but with different values of 23 and 31 meV, respectively.

Table 5 summarizes these results. It should be noted that the $\text{Ag}_2\text{O}/\text{CT-TO-Ac}$ composites are more sensitive to the accelerated aging test than the $\text{Ag}_2\text{O}/\text{CT-TA}$ composites—the greatest shift is observed. The shift in the absorption band to shorter wavelengths is known as the “blue shift”. We looked at the possible causes of this blue shift. It is known that annealing causes a significant blue shift in films E_g [67]. The blue shift effect in the thin films after aging occurs when the number of emitted photons increases and thus shortens the wavelength of light relative to the one emitted by the primary film before aging. In addition, thermal aging can cause an interdiffusion of components on each side of the heterointerface. In these composites, the blue shift of the emission cannot be associated with strong compositional fluctuations [68]. Such an effect on the optical properties can only be explained by interactions at very short distances between the constituents of the films without any signs of structural changes detected by XRD. The thin film shows a blue shift due to some structural defects (such as oxygen vacancies) produced during the aging process. The change in E_g is associated with a change in the quality of the crystal structure of the silver oxide films, as shown by the XRD results. It was possible to obtain a blue shift of the energy gap, accompanied by a decrease in the particle size of the composites obtained after tests for accelerated aging [19,56,69].

The refractive indices for Ag_2O films on the CT surface are given in Table 4. The spectra variation of the n for thin Ag_2O films on CT within the 400 nm–1100 nm wavelength range is shown in Figure 13. The refractive indices of the obtained composites are almost constant over the entire range of visible and near-infrared spectra range. The range of n values obtained after accelerated aging shows that they do not lose their suitability for use in optical non-volatile storage devices or for integration into high-efficiency solar cells.

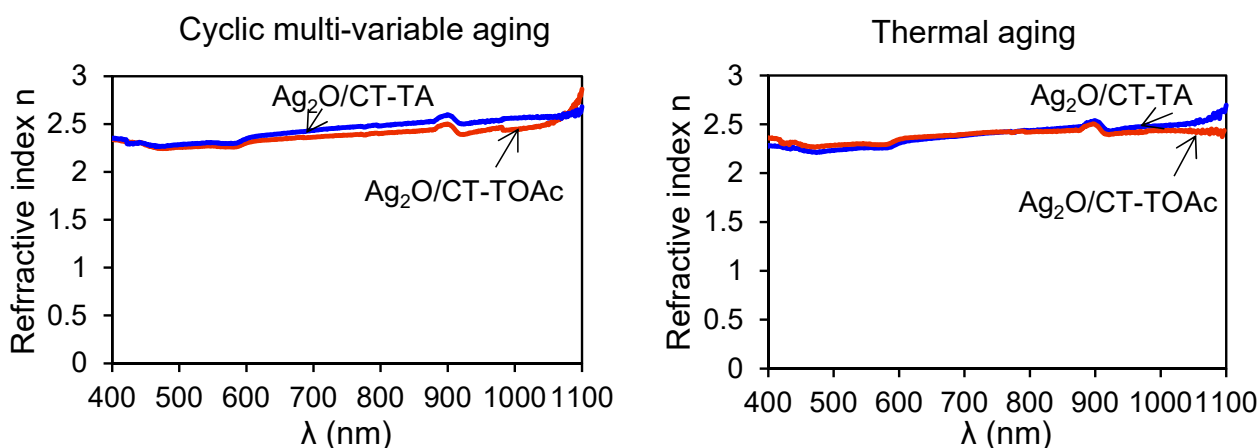


Figure 13. The dependence of refractive indices for Ag_2O films on the CT surface after cyclic multi-variable and thermal aging in terms of wavelength.

3.3. Technical and Mechanical Properties of CT and CT with Ag_2O -Deposited Layer before and after Aging

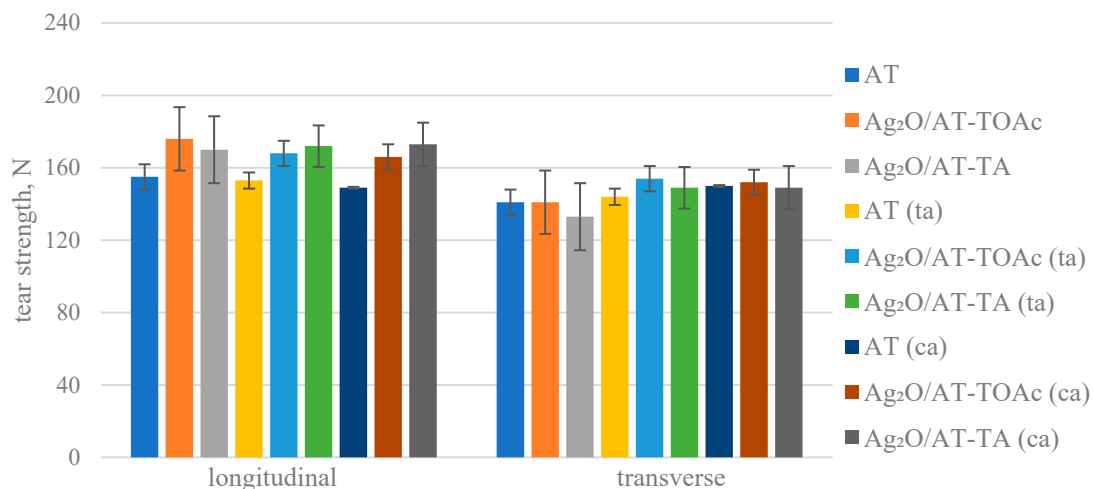
The results (\pm their standard deviation) of the test samples' thickness and total mass per unit area are given in Table 6. It is evident that the relative difference in thickness is negligible (2–4%) for all tested samples, with only a slightly larger variation in the results when the thermochemically treated samples are aged.

Table 6. Results of the initial and thermochemically treated thickness and total mass per unit area before and after aging.

Sample	Before Aging Test		Thermal Aging		Cyclic Multi-Variable Aging	
	<i>T</i> , mm	<i>W</i> , g/mm ²	<i>T</i> , mm	<i>W</i> , g/mm ²	<i>T</i> , mm	<i>W</i> , g/mm ²
CT	0.56 (±0.00)	720 (±6)	0.56 (±0.02)	720 (±6)	0.56 (±0.01)	720 (±8)
Ag ₂ O/CT-TOAc	0.57 (±0.02)	635 (±19)	0.57 (±0.02)	635 (±19)	0.57 (±0.01)	635 (±19)
Ag ₂ O/CT-TA	0.58 (±0.02)	710 (±15)	0.58 (±0.03)	705 (±22)	0.58 (±0.02)	710 (±20)

The situation with the mass characteristic is slightly different. The 12% difference in total mass per unit area between the initial and Ag₂O/CT-TOAc samples is too large to make it possible to state that the treatment did not affect the technical properties of the construction textile. In all cases, aging did not significantly reduce the mass of the samples.

When considering various external factors, such as wind strength, snowfall, mechanical stress, etc., it can be seen that the loads that are being applied to the membrane structures during operation must be mainly withstood by the base of the coated material (the textile-reinforcing component). The physical properties of the material depend upon the polymeric coating with which the material is coated, and this bonding component (matrix) in terms of the composite acts to redistribute the load. When changing the coating surface, it may be the case that the modification processes, as well as the penetration of chemicals into the deeper layers, will act to damage the textile yarns, and the material will lose its strength properties. Mechanical studies have shown that different effects are produced through thermochemical treatment when it comes to changes in cracking and tensile properties. The results showed that the tear strength of both acid-treated and alkali-treated samples did not change (Figure 14). Furthermore, neither thermal nor cyclic multivariable aging had a significant effect on the tear change of either the initial or chemically treated specimens.

**Figure 14.** Tear strength results of initial and thermo-chemically treated CT before and after thermal (ta) and cyclic multi-variable (ca) aging.

The tensile strength results of initial, Ag₂O/CT-TOAc, and Ag₂O/CT-TA before and after aging are presented in Figure 14. The tensile strength of the non-aged test samples was reduced by approximately 28% in both directions due to the processes involved in the surface modification (Figure 15).

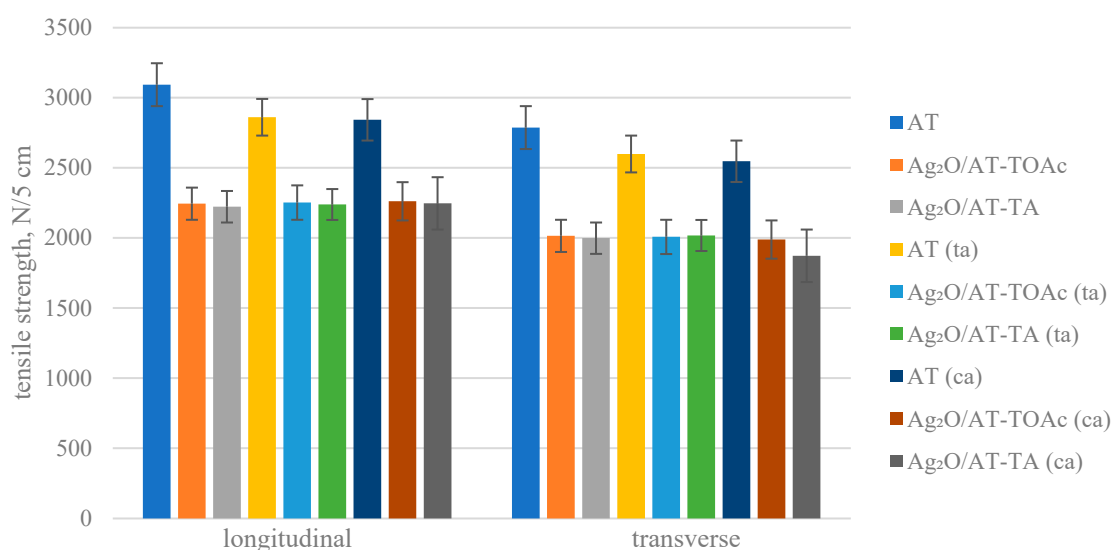


Figure 15. Tensile strength results of initial and thermo-chemically treated CT before and after thermal (ta) and cyclic multi-variable (ca) aging.

Thus, constructional textiles after thermochemical treatment could be damaged more easily under tensile stress than when untreated. The effects of heat, cold, and humidity applied during the aging test did not have a greater impact on the decrease in tensile strength; approximately the same decreasing trend (20–26%) remained. The work of other researchers has shown that depending on the procedures and conditions of the artificial aging test, the values of strength characteristics can vary in a very wide range, from a statistically insignificant change to approximately 30% [32,33,37].

The analysis of failure modes in terms of the initial and thermochemically modified samples during uniaxial stretching revealed that this mode had changed (Figure 16). As for the failure of the initial specimens, this failure produced an even fracture, indicating that the bond between the reinforcing and bonding composite material is sufficiently strong. Due to increasing load, the threads in the material start cracking; failure spreads when stress concentrations are transferred to the adjacent threads. Following the appropriate levels of modification, the failure mode changed to composite failure; i.e., intermediate zones appeared in which the strong bond was lost between the reinforcing composite element and the binding material. As long as the external load is light, such areas are concentrated in a small area and do not spread to where the connection is stronger. As the load increases, the areas gradually increase until a fracture occurs across the entire section. During the accumulation of failures, weak threads gradually go missing, one-piece threads become continuous, and threads of different lengths are pulled in a cross-section.

The influence of various factors is evaluated through the strength reduction factor, at [70], which, together with the safety factor, is recommended as it should be included in structural design calculations, therefore increasing the structural safety limit, which would not be exceeded if the building entered a critical condition (such as due to aging or high-temperature effects, etc.). During the study, it was found that after modifying the construction textile surface with thin silver oxide films, the A_t factor was found to be equal to 1.4. It decreased after thermal and cyclic multi-variable aging (Table 7).

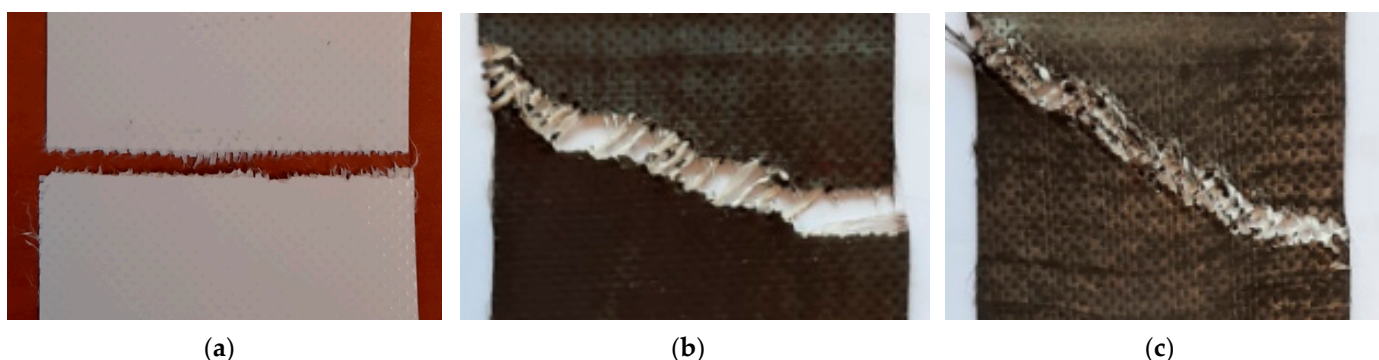


Figure 16. Failure modes for CT (a), Ag₂O/CT-TOAc (b), and Ag₂O/CT-TA (c) samples in tensile tests.

Table 7. Values of the reduction factor A_t of modified CT before and after accelerated aging.

Sample	Before Aging Test	Thermal Aging	Cyclic Multi-Variable Aging
Ag ₂ O/CT-TOAc	1.4/1.4 *	1.3/1.3	1.3/1.3
Ag ₂ O/CT-TA	1.4/1.4	1.3/1.3	1.3/1.4

* in longitudinal/transverse direction.

When comparing the results obtained in the work of other researchers, it can be seen that this coefficient for materials and fused joints, the strength of which varies due to the influence of climatic factors, is $A_t = 1.1$. Therefore, the strength reduction factor of alkali-etched and acid-etched construction textiles with a deposited Ag₂O layer tends to be higher.

Silver oxide is only harmful if swallowed or inhaled as a powder. On the contrary, [71] reported on the use of Ag₂O films as bactericidal coatings. The coatings demonstrated strong adhesion to many substrate materials and impeded the growth of bacteria *Escherichia coli* and *Staphylococcus aureus*, demonstrating a clear zone of inhibition against bacteria growing on solid media and the ability to rapidly inhibit bacterial growth in planktonic culture. Additionally, the coatings exhibited very high elution of silver ions depending on the media conditions. Taken together, the AgO/Ag₂O coatings were effective in eliciting antibacterial activity and have the potential for application on a wide variety of surfaces and devices [71]. From an economic point of view, the preparation of silver oxide coatings usually includes the following elements. First, the choice of the preparation method. Second, the choice of raw materials. Third, control of the reaction conditions, which involves the regulation of the characteristics of the prepared material by adjusting the temperature, reaction time, and other parameters. Among these processes, the choice of preparation method has the greatest influence. The deposition of the Ag₂O layers by our chosen chemical methods pays off the cost of purchasing raw materials, since these methods proceed under standard conditions and do not require complex equipment and costs for their operation. In the future, it is planned to study the possibility of applying silver oxide to building fabrics using the green biosynthesis method. Biosynthesis involves the use of green technology, such as micro-organisms, animals' chitin, seeds, and crude extracts from leaves of plants [72,73]. This method of synthesis is free of toxins, cost-effective, and environmentally friendly. From a practical point of view of using construction textiles, it is relevant that the strength reduction factor of thermochemically modified textiles does not change by a critical amount after aging.

4. Conclusions

The thin silver oxide films, which can be found on various pre-treated PET/PVC construction textiles, were synthesized using the SILAR method. XRD analysis showed that the deposited films are a polycrystalline mixed-phase material consisting of Ag₂O,

AgO, and metallic Ag. The optical properties of the obtained composites were studied using diffuse reflectance spectroscopy in the ultraviolet and visible ranges. From the optical characterization, Ag₂O/CT composite was a direct-gap semiconductor. E_g was found to be 0.89 ± 0.02 eV. The E_g and refractive indices of the composites implied that the samples provided a good source of material for flexible optical applications.

The results obtained show that the tests applied for accelerated aging affect the optical properties of the film. Aging tests caused a blue shift in the optical band gap. It has been established that even after accelerated aging, synthesized composites remain a good material for photovoltaic applications.

The technical properties of the PET/PVC construction textile were not negatively affected by the thermochemical treatment or by the thermal and cyclic multi-variable aging. No appreciable change in tear strength was observed in both directions of the samples after fabric surface modification by thin silver oxide film. Slightly different results were obtained by analyzing the tensile strength of the PET/PVC construction textile. Here, it was determined that, due to the effects being wrought by alkaline and oxidative-acidic treatment, the tensile strength of the construction textiles decreased by up to ~28% in both directions. In addition, analysis of tensile failure modes revealed that a different pattern of cracking occurred in modified samples if a comparison were to be made with untreated samples, thereby indicating a loss of bonding between the reinforcing composite element and the binder. The aforementioned trends in mechanical characteristics remain even after aging according to different factors.

Author Contributions: Conceptualization V.K., V.D. and M.J.; methodology, V.K., V.D. and M.J.; investigation, V.K., V.D. and M.J.; writing—original draft preparation, V.K., V.D. and M.J.; writing—review and editing, V.K., V.D. and M.J. All authors have read and agreed to the published version of the manuscript.

Funding: This research received no external funding.

Institutional Review Board Statement: Not applicable.

Informed Consent Statement: Not applicable.

Data Availability Statement: The data presented in this study are available on request from the corresponding author.

Conflicts of Interest: The authors declare no conflict of interest.

References

1. Paech, C. Structural Membranes Used in Modern Building Facades. *Procedia Eng.* **2016**, *155*, 61–70. [CrossRef]
2. Li, Q.; Zanelli, A. A review on fabrication and applications of textile envelope integrated flexible photovoltaic systems. *Renew. Sustain. Energy Rev.* **2021**, *139*, 110678. [CrossRef]
3. Khan, A.; Hussain, M.; Nur, O.; Willander, M. Fabrication of zinc oxide nanoneedles on conductive textile for harvesting piezoelectric potential. *Chem. Phys. Lett.* **2014**, *612*, 62–67. [CrossRef]
4. Jalil, W.D.A. Smart textiles for the architectural façade. *IOP Conf. Ser. Mater. Sci. Eng.* **2020**, *737*, 012078. [CrossRef]
5. Jia, H.; Cheng, X.; Zhu, J.; Li, Z.; Guo, J. Mathematical and experimental analysis on solar thermal energy harvesting performance of the textile-based solar thermal energy collector. *Renew. Energy* **2018**, *129*, 553–560. [CrossRef]
6. Krylova, V.; Milbrat, A.; Embrechts, A.; Baltrusaitis, J. Ag₂S deposited on oxidized polypropylene as composite material for solar light absorption. *Appl. Surf. Sci.* **2014**, *301*, 134–141. [CrossRef]
7. Zhu, J.; Jia, H.; Cheng, X.; Huang, X.; Liu, X.; Guo, J. The design and performance evaluation of a high-efficient flexible solar air heater based on transparent spacer fabric composite. *Sol. Energy Mater. Sol. Cells* **2019**, *201*, 110089. [CrossRef]
8. Lim, K.H.; Wong, K.W.; Liu, Y.; Zhang, Y.; Cadavid, D.; Cabot, A.; Ng, K.M. Critical role of nano-inclusions in silver selenide nanocomposites as a promising room temperature thermoelectric material. *J. Mater. Chem. C* **2019**, *7*, 2646–2652. Available online: <https://pubs.rsc.org/en/content/articlelanding/2019/TC/C9TC00163H> (accessed on 26 January 2023). [CrossRef]
9. Xiong, W.S.; Jiang, Y.; Xia, Y.; Qi, Y.; Sun, W.; Hu, C.L.; He, R.X.; Chen, B.; Liu, Y.; Zhao, X.Z. A sustainable approach for scalable production of α -Fe₂O₃ nanocrystals with 3D interconnected porous architectures on flexible carbon textiles as integrated electrodes for lithium-ion batteries. *J. Power Sources* **2018**, *401*, 65–72. [CrossRef]
10. Zhang, R.; Liu, J.; Guo, H.; Tong, X. Hierarchically porous nickel oxide nanoflake arrays grown on carbon cloth by chemical bath deposition as superior flexible electrode for supercapacitors. *Mater. Lett.* **2014**, *136*, 198–201. [CrossRef]

11. Pejova, B.; Najdoski, M.; Grozdanov, I.; Dey, S.K. Chemical bath deposition of nanocrystalline (111) textured Ag₂Se thin films. *Mater. Lett.* **2000**, *43*, 269–273. [CrossRef]
12. Krylova, V.; Dukštienė, N.; Lelis, M.; Tučkutė, S. PES/PVC textile surface modification by thermo-chemical treatment for improving its hydrophilicity. *Surf. Interfaces* **2021**, *25*, 101184. [CrossRef]
13. Jatautė, L.; Krylova, V.; Dukštienė, N.; Lelis, M.; Tučkutė, S. Ag-In-Se films on flexible architectural textiles as efficient material for optoelectronics applications: A preliminary study. *Thin Solid Films* **2021**, *721*, 138566. [CrossRef]
14. Pérez-Tomás, A.; Mingorance, A.; Tanenbaum, D.; Lira-Cantú, M. Metal oxides in photovoltaics: All-oxide, ferroic, and perovskite solar cells. In *The Future of Semiconductor Oxides in Next-Generation Solar Cells*; Lira-Cantu, M., Ed.; Elsevier: Amsterdam, The Netherlands, 2018; pp. 267–356. [CrossRef]
15. Cudennec, Y.; Lecerf, A.; Gérard, Y. Synthesis of Cu(OH)₂ and CuO by soft chemistry. *Eur. J. Solid State Inorg. Chem.* **1995**, *32*, 1013–1022.
16. Cudennec, Y.; Lecerf, A. The transformation of Cu(OH)₂ into CuO, revisited. *Solid State Sci.* **2003**, *5*, 1471–1474. [CrossRef]
17. Biemann, M.; Schwaller, P.; Ruffieux, P.; Groning, O.; Schlapbach, L.; Groning, P. AgO investigated by photoelectron spectroscopy: Evidence for mixed valence. *Phys. Rev. B* **2002**, *65*, 235431. [CrossRef]
18. Garner, W.E.; Reeves, L.W. The thermal decomposition of silver oxide. *J. Chem. Soc. Faraday Trans.* **1954**, *50*, 254–260. [CrossRef]
19. Nwanya, A.C.; Ugwuoke, P.E.; Ezekoye, B.A.; Osuji, R.U.; Ezema, F.I. Structural and optical properties of chemical bath deposited silver oxide thin films: Role of deposition time. *Adv. Mater. Sci. Eng.* **2013**, *23*, 450820. [CrossRef]
20. Wei, W.; Mao, X.; Ortiz, L.A.; Sadoway, D.R. Oriented silver oxide nanostructures synthesised through a template-free electrochemical route. *J. Mater. Chem.* **2011**, *21*, 432–438. [CrossRef]
21. Raju, N.R.C.; Kumar, K.J. Photodissociation effects on pulsed laser deposited silver oxide thin films: Surface-enhanced resonance Raman scattering. *J. Raman. Spectrosc.* **2011**, *42*, 1505–1509. [CrossRef]
22. Mehdi, H.E.; Hantehzadeh, M.R.; Valedbagi, S. Physical properties of silver oxide thin film prepared by DC magnetron sputtering: Effect of oxygen partial pressure during growth. *J. Fusion Energ.* **2013**, *32*, 28–33. [CrossRef]
23. Hammad, A.H.; Abdel-Wahab, M.S.; Alshahrie, A. Structural and morphological properties of sputtered silver oxide thin films: The effect of thin film thickness. *Dig. J. Nanomater. Biostructures* **2016**, *11*, 1245–1252.
24. Saroja, G.; Vasu, V.; Nagarani, N. Optical studies of Ag₂O thin film prepared by electron beam evaporation method. *Open J. Met.* **2013**, *3*, 57–63. [CrossRef]
25. Fortiu, E.; Weichman, F.L. Photoconductivity in Ag₂O. *Phys. Stat. Sol. B* **1964**, *5*, 515–524. [CrossRef]
26. Lund, E.; Galeckas, A.; Azarov, A.; Monakhov, E.V.; Svensson, B.G. Photoluminescence of reactively sputtered Ag₂O films. *Thin Solid Films* **2013**, *536*, 156–159. [CrossRef]
27. Ratnayake, S.P.; Ren, J.; Colusso, E.; Guglielmi, M.; Martucci, A.; Gaspera, E.D. SILAR deposition of metal oxide nanostructured films. *Small* **2021**, *17*, 2101666. [CrossRef] [PubMed]
28. Karoro, A.; Nuru, Z.Y.; Kotsedi, L.; Bouziane, K.; Mothudi, B.M.; Maaza, M. Laser nanostructured Co nanocylinders-Al₂O₃ cermet for enhanced & flexible solar selective absorbers applications. *Appl. Surf. Sci.* **2015**, *347*, 679–684. Available online: <https://www.sciencedirect.com/science/article/pii/S0169433215009484> (accessed on 1 February 2023).
29. Kozlovskiy, A.; Zdorovets, M.; Kenzhina, I.; Berguzinov, A.; Tishkevich, D.; Zubar, T.; Trukhanov, A. The study of the applicability of ionizing radiation to increase the photocatalytic activity of TiO₂ thin films. *J. Nanostructure Chem.* **2020**, *10*, 331–346. [CrossRef]
30. Jelle, B.P. Accelerated climate ageing of building materials, components and structures in the laboratory. *J. Mater. Sci.* **2012**, *47*, 6475–6496. [CrossRef]
31. Shang, Y.; Yang, B.; Wu, M.; Tao, Y.; Qin, J. Degradation of PVDF-Coated fabrics after engineering applications: Correlations between surface microstructure, physical properties, and mechanical properties based on statistical analysis. *Adv. Polym. Technol.* **2021**, *2021*, 9345451. [CrossRef]
32. Yang, B.; Yang, Y.; Huo, Z.; Yu, Y. Advances in research on aging properties of polyvinyl chloride and polyvinylidene fluoride membranes. *Constr. Build. Mater.* **2023**, *367*, 130292. [CrossRef]
33. Sacevičienė, V.; Jucienė, M.; Dobilaitė, V.; Krylova, V.; Žalėnienė, S.; Dukštienė, N.; Bliūdžius, R. Investigation of the changes in physical properties of PES/PVC fabrics after aging. *Inc. J. Appl. Polym. Sci.* **2019**, *136*, 47523. [CrossRef]
34. Asadi, H.; Uhlemann, J.; Stranghoener, N.; Ulbricht, M. Tensile strength deterioration of PVC coated PET woven fabrics under single and multiplied artificial weathering impacts and cyclic loading. *Constr. Build. Mater.* **2022**, *342*, 127843. [CrossRef]
35. Li, Y.; Liu, T.; Yang, B.; Zhang, Q.; Zhang, Y. Effects of natural ageing on mechanical properties of PVDF-coated fabrics. *Struct. Eng. Int.* **2016**, *26*, 348–356. [CrossRef]
36. Ducoulombier, L.; Dakhli, Z.; Lafhaj, Z. Durability of textile facing materials for construction: Implementation of an accelerated aging test by hydrolysis. *J. Ind. Text.* **2016**, *45*, 1288–1307. [CrossRef]
37. Yang, X.; Jiang, X.; Hu, J.; Wang, F.; Hu, C. Relationship between physical and mechanical properties of accelerated weathering and outdoor weathering of PVC-coated membrane material under tensile stress. *J. Ind. Text.* **2016**, *47*, 197–210. [CrossRef]
38. Zhang, Y.; Zhang, M. Aging Properties of Polyvinylidene fluoride-Coated polyesters used in tensioned membrane structure: Effect of loading protocol and environment. *Adv. Mater. Sci. Eng.* **2017**, *2017*, 8789247. [CrossRef]
39. Mazrouei-Sebdani, Z.; Khoddami, A. Alkaline hydrolysis: A facile method to manufacture superhydrophobic polyester fabric by fluorocarbon coating. *Prog. Org. Coat.* **2011**, *72*, 638–646. [CrossRef]

40. Fiore, V.; Di Bella, G.; Valenza, A. The effect of alkaline treatment on mechanical properties of kenaf fibers and their epoxy composites. *Compos. Part B Eng.* **2015**, *68*, 14–21. [[CrossRef](#)]
41. Lin, J.; Yang, Z.; Hu, X.; Hong, G.; Zhang, S.; Song, W. The effect of alkali treatment on properties of dopamine modification of bamboo fiber/poly(lactic acid) composites. *Polymers* **2018**, *10*, 403. [[CrossRef](#)]
42. Alaburdaite, R.; Krylova, V. Study of thermo-oxidative chemical pre-treatment of isotactic polypropylene. *J. Therm. Anal. Calorim.* **2014**, *118*, 1331–1338. [[CrossRef](#)]
43. Holleman, A.F.; Wiberg, E.; Wiberg, W. *Inorganic Chemistry*; Academic Press: San Diego CA, USA, 2001; p. 136.
44. *ISO 1419*; Rubber- or Plastics-Coated Fabrics—Accelerated-Ageing Tests. Lithuanian Standards Board (LST): Vilnius, Lithuania, 2019.
45. *ISO 2286-3*; Rubber- or Plastics-Coated Fabrics—Determination of Roll Characteristics—Part 3: Method for Determination of Thickness. Lithuanian Standards Board (LST): Vilnius, Lithuania, 2016.
46. *ISO 2286-2*; Rubber- or Plastics-Coated Fabrics—Determination of Roll Characteristics Methods for Determination of Total Mass per Unit Area, Mass per Unit Area of Coating and Mass per Unit Area of Substrate. Lithuanian Standards Board (LST): Vilnius, Lithuania, 2016.
47. *ISO 1421*; Rubber- or Plastics-Coated Fabrics—Determination of Tensile Strength and Elongation at Break. Lithuanian Standards Board (LST): Vilnius, Lithuania, 2016.
48. *EN 1875-3*; Rubber- or Plastics-Coated Fabrics—Determination of Tear Strength-Part 3: Trapezoidal Method (Five-Highest-Peak Calculation). Lithuanian Standards Board (LST): Vilnius, Lithuania, 2023.
49. *ISO 2231*; Rubber- or Plastics-Coated Fabrics—Standard Atmospheres for Conditioning and Testing. Lithuanian Standards Board (LST): Vilnius, Lithuania, 1995.
50. Rajabi, A.; Ghazali, M.J.; Mahmoudi, E.; Baghdadi, A.H.; Mohammad, A.W.; Mustafah, N.M.; Ohnmar, H.; Naicker, A.S. Synthesis, characterization, and antibacterial activity of Ag₂O-loaded polyethylene terephthalate fabric via ultrasonic method. *Nanomaterials* **2019**, *9*, 450. [[CrossRef](#)] [[PubMed](#)]
51. Al Sarraj, A.; Saoud, K.M.; Elmel, A.; Mansour, S.; Haik, Y. Optoelectronic properties of highly porous silver oxide thin film. *SN Appl. Sci.* **2021**, *3*, 15. [[CrossRef](#)]
52. Taufik, A.; Saleha, R. The influence of graphene on silver oxide synthesis through microwave assisted method. *AIP Conf. Proc.* **2023**, *2018*, 020018-1–020018-4. [[CrossRef](#)]
53. Valverde-Aguilar, G.; Garcia-Macedo, J.A.; Rentería-Tapia, V. Silver core—Silver oxide shell nanoparticles embedded on mesostructured silica films. *J. Nano Res.* **2008**, *3*, 103–114. [[CrossRef](#)]
54. Lopez, R.; Gomez, R. Band-gap energy estimation from diffuse reflectance measurements on sol-gel and commercial TiO₂: A comparative study. *J. Sol. Gel Sci. Technol.* **2012**, *61*, 1–7. [[CrossRef](#)]
55. Nasr, M.; Viter, R.; Eid, C.; Warmont, F.; Habchi, R.; Miele, P.; Bechelany, M. Synthesis of novel ZnO/ZnAl₂O₄ multi co-centric nanotubes and their long-term stability in photocatalytic application. *RSC Adv.* **2016**, *6*, 103692–103699. [[CrossRef](#)]
56. Raju, N.R.C.; Kumar, K.J.; Subrahmanyam, A. Physical properties of silver oxide thin films by pulsed laser deposition: Effect of oxygen pressure during growth. *J. Phys. D.* **2009**, *42*, 135411. [[CrossRef](#)]
57. Ramesh, M.N.V.; Sundarayya, Y.; Sunandana, C.S. Reactively radio frequency sputtered silver oxide thin films: Phase evolution and phase stability. *Mod. Phys. Lett. B* **2007**, *21*, 1933–1944. [[CrossRef](#)]
58. Raj, K.R.; Murugakoothan, P. Studies on the optical and mechanical properties of non-linear optical 3-aminophenol orthophosphoric acid (3-amphph) single crystal. *Optik* **2012**, *123*, 1082–1086. [[CrossRef](#)]
59. Grothe, J.; Kaskel, S.; Leuteritz, A. 8.08—Nanocomposites and hybrid materials. *Polym. Sci. A Compr. Ref.* **2012**, *8*, 177–209. [[CrossRef](#)]
60. Zhang, X.; Qiu, J.; Zhao, J.; Li, X.; Liu, L. Complex refractive indices measurements of polymers in infrared bands. *J. Quant. Spectrosc. Radiat. Transf.* **2020**, *252*, 107063. [[CrossRef](#)]
61. Hinrichs, K.; Eichhorn, K.J. Combined infrared and visible spectroscopic ellipsometry study of thin polymer layers. *Spectrosc. Eur.* **2007**, *19*, 11–14.
62. Biron, M. *Thermoplastics and Thermoplastic Composites*, 2nd ed.; William Andrew: Norwich, NY, USA, 2013.
63. Utry, N.; Ajtai, T.; Pintér, M.; Tombác, E.; Illés, E.; Bozóki, Z.; Szabó, G. Mass-specific optical absorption coefficients and imaginary part of the complex refractive indices of mineral dust components measured by a multi-wavelength photoacoustic spectrometer. *Atmos. Meas. Tech.* **2015**, *8*, 401–410. [[CrossRef](#)]
64. Ghosh, G. Dispersion-equation coefficients for the refractive index and birefringence of calcite and quartz crystals. *Opt. Commun.* **1999**, *163*, 95–102. [[CrossRef](#)]
65. Goodman, A.M. Optical interference method for the approximate determination of refractive index and thickness of a transparent layer. *Appl. Opt.* **1978**, *17*, 2779–2787. [[CrossRef](#)]
66. Kisi, E.H.; Howard, C.J. *Applications of Neutron Powder Diffraction*; Oxford University Press: Oxford, UK, 2008; pp. 134–191. [[CrossRef](#)]
67. Kasanaboina, P.; Sharma, M.; Deshmukh, P.; Reynolds, C.; Liu, Y.; Iyer, S. Effects of Annealing on GaAs/GaAsSbN/GaAs core-multi-shell nanowires. *Nanoscale Res. Lett.* **2016**, *11*, 25277267. [[CrossRef](#)]
68. Roy, S.C.; Sharma, G.L.; Bhatnagar, M.C. Large blue shift in the optical band-gap of sol-gel derived Ba_{0.5}Sr_{0.5}TiO₃ thin films. *Solid State Commun.* **2007**, *141*, 243–247. [[CrossRef](#)]

69. Thomas, R.; Dube, D.C.; Kamalasanan, M.N.; Chandra, S. Optical and electrical properties of BaTiO₃ thin films prepared by chemical solution deposition. *Thin Solid Films* **1999**, *346*, 212–225. [[CrossRef](#)]
70. Stranghöner, N.; Uhlemann, J.; Bilginoglu, F.; Bletzinger, K.U.; Bögner-Balz, H.; Corne, E.; Gibson, N.; Gosling, P.; Houtman, R.; Llorens, J.; et al. *Prospect for European Guidance for the Structural Design of Tensile Membrane Structures Support to the Implementation, Harmonization and Further Development of the Eurocodes*; EUR—Scientific and Technical Research Reports No. EUR 27716 EN; Publications Office of the European Union: Luxembourg, 2016.
71. Goderecci, S.S.; Kaiser, E.; Yanakas, M.; Norris, Z.; Scaturro, J.; Oszust, R.; Medina, C.D.; Waechter, F.; Heon, M.; Krchnavek, R.R.; et al. Silver oxide coatings with high silver-ion elution rates and characterization of bactericidal activity. *Molecules* **2017**, *22*, 1487. [[CrossRef](#)]
72. Aisida, S.O.; Ugwu, K.C.; Akpa, P.A.; Nwanya, A.C.; Nwankwo, U.O.; Botha, S.; Ejikeme, P.M.; Ahmad, I.; Maaza, M.; Ezema, F.I. Biosynthesis of silver nanoparticles using bitter leave (*Veronica amygdalina*) for antibacterial activities. *Surf. Interfaces* **2019**, *17*, 100359. Available online: <https://repository.uwc.ac.za/handle/10566/8274?show=full> (accessed on 15 February 2023). [[CrossRef](#)]
73. Khalil, A.T.; Ovais, M.; Ullah, I.; Ali, M.; Jan, S.A.; Shinwari, Z.K. Bioinspired synthesis of pure massicot phase lead oxide nanoparticles and assessment of their biocompatibility, cytotoxicity and in-vitro biological properties. *Arab. J. Chem.* **2020**, *13*, 916–931. Available online: <https://www.sciencedirect.com/science/article/pii/S187853521730165X?via%3Dihub> (accessed on 7 September 2023). [[CrossRef](#)]

Disclaimer/Publisher’s Note: The statements, opinions and data contained in all publications are solely those of the individual author(s) and contributor(s) and not of MDPI and/or the editor(s). MDPI and/or the editor(s) disclaim responsibility for any injury to people or property resulting from any ideas, methods, instructions or products referred to in the content.